Extremely large dynamics of axially excited cantilevers

Mergen H. Ghayesh [a,*], Hamed Farokhi [b]

[a] *School of Mechanical Engineering, University of Adelaide, South Australia 5005, Australia*
[b] *Department of Mechanical and Construction Engineering, Northumbria University, Newcastle upon Tyne NE1 8ST, UK*
**Corresponding author: mergen.ghayesh@adelaide.edu.au*
Email: (H Farokhi): hamed.farokhi@northumbria.ac.uk

Abstract

The nonlinear parametric resonance of a cantilever under axial base excitation is examined while capturing extremely large oscillation amplitudes for the first time. A geometrically exact model is developed for the cantilever based on the Euler-Bernoulli beam theory and inextensibility condition. In order to be able to capture extremely large oscillation amplitudes accurately, the equation of motion is derived for centreline rotation while keeping trigonometric terms intact. The developed model is verified for the static case through comparison to a three-dimensional nonlinear finite element model. The internal energy dissipation model of Kelvin-Voigt is used to model the system damping in large amplitudes more accurately. The Galerkin modal decomposition scheme is utilised for discretisation procedure while keeping the trigonometric terms intact. It is shown that in parametric resonance region, the oscillation amplitudes grow extremely large even for smallest possible amplitudes of the base excitation, which highlights the significant importance of employing a geometrically exact model to examine the parametric resonance response of a cantilever.

Keywords: Cantilever; Parametric resonance; Extremely large oscillation; Kelvin-Voigt; Geometrically exact model

1. Introduction

Beams, subject to dynamic loads, are one of the common thin-walled structures which play an important role in different machines and structures [1-6]. Cantilevers, among beams, under direct or parametric excitation are present in many engineering systems and applications [7, 8]. In particular, cantilevers are present in scanning probe microscopy, mass and bio sensors, micro/nano-electromechanical systems, and energy harvesters [9-12]. Presence of various sources of nonlinearities, such as geometric nonlinearities arising from large rotation and inertial nonlinearities due to relationship between axial and transverse displacements through the inextensibility condition, makes the nonlinear dynamical analysis of such systems a challenging task. The present study will not provide a very detailed review of the literature, but rather highlights the main reason for developing of a new model for analysis of parametric resonance of cantilevers.

A lot of studies have been conducted over the past few decades on examining the nonlinear static and dynamic behaviours of cantilevers. For instance, Crespo da Silva and Glynn [13, 14] obtained the equations of motion of inextensional beams taking into account geometric and inertial nonlinearities; they analysed the equations via the method of multiple scales. Nayfeh and Pai [15, 16] examined the nonlinear out-of-plane vibrations of a cantilever under lateral base excitation. Further investigations were conducted for instance by Feng and Leal [17], Anderson et al. [18], Hamdan and Dado [19], Arafat et al. [20], and Esmailzadeh and Jalili [21]. More recently, Farokhi et al. [22] utilised a high-dimensional model to demonstrate the effect of various sources of nonlinearity in a vibrating cantilever; they showed that both geometric and inertial nonlinearities have significant effect on resonance response of a vibrating cantilever and that neglecting either of those

nonlinearities lead to very inaccurate results. Additionally, many studies have been performed on the application of cantilevers in energy harvesting [9-12, 23-25].

In all the valuable studies on parametric resonance of cantilevers, the equations of motion are obtained for the transverse and longitudinal or only the transverse motion. Throughout the derivation procedure of the equation of motion of a cantilever under inextensibility condition, the following equation is commonly used: $\theta = \sin^{-1}(\partial w/\partial x)$. This equation implies that the tip angle varies only between $\pm 90°$; in other words, the transverse equation of motion of a cantilever fails to predict system response if the tip angle grows larger than 90°. This limitation is easily reached for cantilevers under axial base excitation in which the oscillation amplitude in the parametric resonance region grows rapidly. This limitation can be overcome by deriving the equation of motion of a cantilever for the centreline rotation.

The present study for the first time examines the nonlinear parametric resonance of a cantilever undergoing extremely large oscillation amplitudes. To this end, a geometrically exact model is developed through deriving the equation of motion for the rotation of the centreline of the cantilever while keeping all trigonometric terms intact in the derivation procedure (as detailed in Section 2). The developed model is verified for a static case via comparison to a three-dimensional nonlinear finite element model (as explained in Section 3). The numerical results are presented for two cases, with either the frequency or amplitude of the base exaction varying as the bifurcation parameter (as detailed in Section 4).

2. Model development

The system examined in this study is a cantilever with a tip mass under axial base excitation as shown in Fig. 1. Two coordinate systems are shown on the beam, i.e. *XZ* and *xz*, denoting the inertial and curvilinear coordinates, respectively. The cantilever is under axial base excitation (in the *X* direction) of $x_0\sin(\omega_0 t)$, with x_0 denoting the base excitation amplitude while ω_0 shows the frequency of the excitation. The thickness, width, and length of the cantilever are represented respectively by *h*, *b*, and *L*, respectively.

Inextensibility assumption indicates that the length of the centreline remains constant during oscillation. This assumption, which is a well-known assumption in modelling of cantilevers, is utilised in this study. It is important to note that under the inextensibility condition, the length of an element of the beam before and after deformation remains the same. Another outcome of the inextensibility assumption is that it reduces the independent displacements of the system to one. Hence, the displacements in the transverse, $w(x,t)$, and axial, $u(x,t)$, directions can be written in terms of the centreline rotation angle $\theta(x,t)$. This is expressed as

$$\begin{aligned} w(x,t) &= \int_0^x \sin\left[\theta(\xi,t)\right]\mathrm{d}\xi, \\ u(x,t) &= -\int_0^x \left(1-\cos\left[\theta(\xi,t)\right]\right)\mathrm{d}\xi. \end{aligned} \tag{1}$$

One important note should be emphasised here again; the reason for writing the cantilever displacements in terms of the centreline rotation is that it allows deriving the cantilever motion equation in terms of θ. The main advantage of this compared to an equation for the

transverse motion is that it is capable of predicting the cantilever response even when the tip angle grows larger than 90°.

Knowing that u in Eq. (1) denotes the axial displacement relative to the base, the total axial displacement can be formulated as

$$u_T(x,t) = x_0 \sin(\omega_0 t) - \int_0^x \left(1 - \cos\left[\theta(\xi,t)\right]\right) \mathrm{d}\xi. \tag{2}$$

Taking into account the rotational inertia, the kinetic energy of the cantilever, while under axial base-excitation, can be derived as

$$\begin{aligned} K = \frac{1}{2}\int_0^L \left[\rho A + M_0 \delta_D(x-L)\right] \Bigg\{ \Bigg[x_0\omega_0 \cos(\omega_0 t) - \int_0^x \frac{\partial\theta(\xi,t)}{\partial t} \sin\left(\theta(\xi,t)\right) \mathrm{d}\xi \Bigg]^2 \\ + \Bigg[\int_0^x \frac{\partial\theta(\xi,t)}{\partial t} \cos\left(\theta(\xi,t)\right) \mathrm{d}\xi \Bigg]^2 \Bigg\} \mathrm{d}x + \frac{1}{2}\int_0^L \rho I \left(\frac{\partial\theta(x,t)}{\partial t} \right)^2 \mathrm{d}x, \end{aligned} \tag{3}$$

with M_0 and ρ denoting the tip mass and the beam mass density, respectively, and A and I standing for the cross-sectional area and its second moment, respectively; δ_D represents the Dirac delta function, while x_0 and ω_0 denote the base excitation amplitude and frequency, respectively.

The next step is to derive the strain energy of the cantilever. Therefore, the axial strain is first formulated in terms of the centreline rotation as

$$\varepsilon_{xx}(x,z,t) = -z \frac{\partial\theta(x,t)}{\partial x}. \tag{4}$$

The axial stress-strain relationship based on the internal energy dissipative model of the Kelvin-Voigt [26-28] can be formulated as

$$\sigma_{xx}\left(x,z,t\right)=E\varepsilon_{xx}+\mu\frac{\partial\varepsilon_{xx}}{\partial t}, \tag{5}$$

with E and μ respectively denoting the material Young's modulus and viscosity. It should be noted that the first term in Kelvin-Voigt stress contributes to the elastic strain energy while the second term causes dissipation in the system. Hence, the elastic strain energy and the virtual dissipative work are given by

$$U=\frac{1}{2}\int_0^L EI\left[\frac{\partial\theta(x,t)}{\partial x}\right]^2\mathrm{d}x, \tag{6}$$

$$\delta D=-\int_0^L \mu I\left[\delta\left(\frac{\partial\theta(x,t)}{\partial x}\right)\frac{\partial^2\theta(x,t)}{\partial x\partial t}\right]\mathrm{d}x, \tag{7}$$

with δ denoting the variational operator.

The centreline rotation equation of motion can be derived utilising the generalised principle of Hamilton as

$$\begin{aligned}&-\sin\theta\int_L^x\left[\rho A+M_0\delta_D\left(x-L\right)\right]\left\{x_0\omega_0^2\sin\left(\omega_0 t\right)+\int_0^x\left[\left(\frac{\partial\theta}{\partial t}\right)^2\cos\theta+\frac{\partial^2\theta}{\partial t^2}\sin\theta\right]\mathrm{d}x\right\}\mathrm{d}x+\rho I\frac{\partial^2\theta}{\partial t^2}\\&+\cos\theta\int_L^x\left\{\left[\rho A+M_0\delta_D\left(x-L\right)\right]\int_0^x\left[\left(\frac{\partial\theta}{\partial t}\right)^2\sin\theta-\frac{\partial^2\theta}{\partial t^2}\cos\theta\right]\mathrm{d}x\right\}\mathrm{d}x-EI\frac{\partial^2\theta}{\partial x^2}-\mu I\frac{\partial^3\theta}{\partial t\partial x^2}=0,\end{aligned} \tag{8}$$

Defining the following dimensionless quantities

$$\begin{aligned}&\beta=\frac{AL^2}{I}, \qquad x^*=\frac{x}{L}, \qquad t^*=\frac{t}{\tau}, \qquad \gamma=\frac{M_0}{\rho AL}\\&\mu_d=\frac{\mu}{E\tau}, \qquad x_b=\frac{x_0}{L}, \qquad \omega_b=\omega_0\tau,\end{aligned} \tag{9}$$

in which $\tau=L^2\sqrt{\rho A/(EI)}$, the dimensionless equation of motion can be obtained as

$$
\begin{aligned}
&-\sin\theta\int_1^x\left[1+\gamma\delta_D\left(x-1\right)\right]\left\{x_b\omega_b^2\sin\left(\omega_b t\right)+\int_0^x\left[\left(\frac{\partial\theta}{\partial t}\right)^2\cos\theta+\frac{\partial^2\theta}{\partial t^2}\sin\theta\right]\mathrm{d}x\right\}\mathrm{d}x+\frac{1}{\beta}\frac{\partial^2\theta}{\partial t^2}\\
&+\cos\theta\int_1^x\left\{\left[1+\gamma\delta_D\left(x-1\right)\right]\int_0^x\left[\left(\frac{\partial\theta}{\partial t}\right)^2\sin\theta-\frac{\partial^2\theta}{\partial t^2}\cos\theta\right]\mathrm{d}x\right\}\mathrm{d}x-\frac{\partial^2\theta}{\partial x^2}-\mu_d\frac{\partial^3\theta}{\partial t\partial x^2}=0,
\end{aligned}
\tag{10}
$$

where the asterisk symbol is disregarded for convenience.

In what follows, a modal discretisation based on the Galerkin approach is performed to reduce the partial differential-type equation of motion into a set of ordinary differential ones. To this end, the centreline rotation is expanded into a series consisting of time-dependent coordinates (denoted by $p_k(t)$) multiplied by specific shape functions (denoted by $\Delta_k(x)$). The shape function used in this study is given by

$$
\begin{aligned}
&\Delta_k(x)=\left(\sinh\left(\eta_k x\right)-\alpha_k\cosh\left(\eta_k x\right)\right)+\left(\sin\left(\eta_k x\right)+\alpha_k\cos\left(\eta_k x\right)\right),\\
&\alpha_k=\left[\left(\sinh\left(\eta_k\right)+\sin\left(\eta_k\right)\right)^{-1}\right]\left(\cosh\left(\eta_k\right)+\cos\left(\eta_k\right)\right),
\end{aligned}
\tag{11}
$$

in which η_k is the kth root of the equation $\cos(\eta)\cosh(\eta)=-1$. Following the rest of the Galerkin approach procedure gives the discretised equations of motion as

$$
\begin{aligned}
&\frac{1}{\beta}\sum_{k=1}^{Q}\left(\int_0^1\Delta_j\Delta_k\,\mathrm{d}x\right)\ddot{p}_k-\sum_{k=1}^{Q}\left(\int_0^1\Delta_j\Delta_k''\,\mathrm{d}x\right)p_k-\mu_d\sum_{k=1}^{Q}\left(\int_0^1\Delta_j\Delta_k''\,\mathrm{d}x\right)\dot{p}_k\\
&-\int_0^1\Delta_j\left\{\sin\left(\sum_{k=1}^{Q}\Delta_k(x)p_k(t)\right)\int_1^x\left[1+\gamma\delta_D\left(x-1\right)\right]\left(\int_0^x\left[\left(\frac{\partial}{\partial t}\left(\sum_{k=1}^{Q}\Delta_k(x)p_k(t)\right)\right)^2\cos\left(\sum_{k=1}^{Q}p_k(t)\Delta_k(x)\right)\right.\right.\\
&\qquad\left.\left.+\frac{\partial^2}{\partial t^2}\left(\sum_{k=1}^{Q}\Delta_k(x)p_k(t)\right)\sin\left(\sum_{k=1}^{Q}\Delta_k(x)p_k(t)\right)\right]\mathrm{d}x+x_b\omega_b^2\sin\left(\omega_b t\right)\right)\mathrm{d}x\right\}\mathrm{d}x\\
&+\int_0^1\Delta_j\left\{\cos\left(\sum_{k=1}^{Q}\Delta_k(x)p_k(t)\right)\int_1^x\left(\left[1+\gamma\delta_D\left(x-1\right)\right]\int_0^x\left[\left(\frac{\partial}{\partial t}\left(\sum_{k=1}^{Q}\Delta_k(x)p_k(t)\right)\right)^2\sin\left(\sum_{k=1}^{Q}p_k(t)\Delta_k(x)\right)\right.\right.\\
&\qquad\left.\left.-\frac{\partial^2}{\partial t^2}\left(\sum_{k=1}^{Q}\Delta_k(x)p_k(t)\right)\cos\left(\sum_{k=1}^{Q}\Delta_k(x)p_k(t)\right)\right]\mathrm{d}x\right)\mathrm{d}x\right\}\mathrm{d}x=0,\qquad j=1,2,\ldots,Q.
\end{aligned}
\tag{12}
$$

There are several points which should be highlighted and emphasised here. First, the trigonometric terms must be kept intact to guarantee accurate results when the amplitude of oscillation grows very large. More specifically, as will be shown in the numerical results, the tip angle could go as high as π; for such large variations in the centreline angle, the trigonometric terms must be kept as is to ensure accurate predictions. The second point is that when the trigonometric terms are kept intact, the integrations from 0 to x, 1 to x, and 0 to 1 cannot be performed in closed form; hence, these terms are integrated numerically while retaining sufficient number of terms. This procedure results in very large-size equations and hence increases the computational costs, but ensures reliable results even at extremely large oscillation amplitudes. The third point is the number of modes required to obtain converged results. In the present study, Q is set to 6, resulting in 6-degree-of-freedom (DOF) system which is sufficient to obtain converged results. A pseudo-arclength continuation technique is utilised to solve the resultant discretised set of equations numerically, which results in the amplitude of the centreline rotation; the axial and transverse motion amplitudes will then be obtained using the relationship given in Eq. (1).

3. Model verification

The model developed in Section 2 is verified in this section through comparison to three-dimensional (3D) nonlinear finite element analysis (FEA). More specifically, a nonlinear static analysis is performed on a cantilever subject to a tip load perpendicular to the beam centreline, using the model developed in Section 2 as well as a 3D nonlinear FEA via Abaqus/CAE. The comparison is performed for a cantilever of h=1 mm, L/h=200, and b/h=5. An 8-node quadrilateral continuum shell element with reduced integration is utilised

for its superior accuracy compared to conventional shell elements; a mesh size of 0.5 mm is used to ensure converged results.

The static equation of motion for a cantilever subject to a tip load which is always perpendicular to the beam centreline can be derived as

$$F_{tip}\left[\cos\theta\int_{x}^{1}\left[\cos\theta\,\delta_D(x-1)\right]\mathrm{d}x+\sin\theta\int_{x}^{1}\left[\sin\theta\,\delta_D(x-1)\right]\mathrm{d}x\right]+\frac{\partial^2\theta}{\partial x^2}=0, \tag{13}$$

where $F_{tip}=FL^2/(EI)$, in which F is the dimensional force applied to the tip and F_{tip} is its dimensionless counterpart. The static equation of motion is discretised following the procedure explained in Section 2. The FEA results are made dimensionless as well.

The deformed configurations of the cantilever for three different tip loads are shown in Fig. 2. The symbols indicate the results obtained via 3D nonlinear FEA while the solid line indicates those obtained via the model developed in the present study. As seen, the deformations predicted by the model developed in this study are very close to those of the 3D nonlinear FEA even at extremely large deformation magnitudes. This comparison verifies the accuracy and reliability of the model developed in this study as well as the accuracy of the employed numerical technique. The contour plots of the 3D nonlinear FEA analysis for the most extreme case of Fig. 2, i.e. when F_{tip}=7.24, are shown in Fig. 4 for both transverse and axial deformations.

4. Nonlinear parametric resonance

This section investigates the nonlinear parametric resonance of the cantilever under axial base excitation. It is worth mentioning that a cantilever under axial base excitation is

classified as a parametrically excited system. For such a system, parametric resonance could occur when the frequency of the axial base excitation is varied near twice the fundamental transverse natural frequency. It should be noted that in this section, the nondimensional fundamental transverse natural frequency is shown by ω_1, which is related to its dimensional counterpart $\hat{\omega}_1$ through $\omega_1 = \hat{\omega}_1 \tau$. Two different types of parameter resonance analyses are performed in this section. The first type is by fixing the amplitude of the base excitation and changing its frequency in a range around twice the first transverse natural frequency. The second type of analysis is performed by fixing the frequency of the base excitation to a value near twice the fundamental transverse natural frequency and varying the amplitude of the base excitation as the bifurcation parameter. The results of these analyses are discussed in detail in the following. One important note should be made here regarding the value of β, as it is the only parameter whose value requires defining specific dimensions. For any beam with a large length-to-thickness aspect ratio, the value of β will be large enough so that the term $1/\beta$ can be safely neglected. The reason for emphasising this is that the aim of this study is to present general dimensionless results which are applicable to any cantilever. The value of β=480000 is used in this study which corresponds to a cantilever with L/h=200. But, as long as the cantilever length-to-thickness ratio is large enough (more than 50 for instance), the results of the present study can be used safely. The dimensionless material viscosity coefficient μ_d is set to 0.004 throughout this study. This value of damping is equivalent to a damping ratio of $\zeta = 0.007$ for small oscillations. In all the results presented for parametric resonance cases, the solid line indicates the stable solution while the dashed line shows the unstable one.

4.1 Parametric resonance due to varying base excitation frequency

This section examines the nonlinear parametric resonance of the cantilever when the frequency of the axial base excitation is changed as the bifurcation parameter. The nonlinear parametric resonance response of the cantilever under base excitation is shown in Fig. 4 when x_b=0.005. The frequency-amplitude diagrams are shown for (a, b) tip displacements in transverse and axial directions, respectively, corresponding to maximum tip rotation (c). It is visibly seen that the cantilever shows a hardening-type nonlinear response in parametric resonance region. More specifically, as the frequency is varied near $2\omega_1$, two nontrivial solution branches are bifurcated from the trivial zero-amplitude state via two period-doubling bifurcations at points P_1 and P_2 corresponding to ω_b=1.9932 ω_1 and 2.0072 ω_1, respectively. The two bifurcation solution branches, one stable and one unstable, coincide at point S (ω_b=2.0356 ω_1) corresponding to a saddle-node bifurcation. It is seen that the oscillation amplitude goes as high as almost 80% of the beam length, which highlights the necessity of employing a geometrically exact model.

Increasing the amplitude of the axial base excitation to x_b=0.01 leads to a new set of results as illustrated in Fig. 5. As seen, due to increased base excitation amplitude, the unstable region between the two period-doubling bifurcations becomes wider and the saddle-node bifurcation occurs at a larger excitation frequency. One interesting aspect of the resonance transverse response is that it reaches a local maximum at ω_b=2.0312 ω_1, and then decreases with increasing frequency. This is due to the fact that the transverse displacement plotted here corresponds to maximum tip rotation. The decrease in the transverse displacement amplitude indicates that the cantilever tip has deflected so much that it bends backward. This behaviour is shown in more detail in Fig. 6 through plotting the

oscillation of the cantilever in one period at different excitation frequencies. As seen for the last case, i.e. sub-figure (d), the transverse amplitude of the tip reaches a maximum value and the decreases. One important note should be made here that such extremely large amplitudes can be obtained only using a geometrically exact model while retaining all nonlinearities, i.e. the model developed in Section 2. The significance of a geometrically exact model is better shown in Appendix A through comparison of static and dynamic results to a third-order truncated model. Another important factor is retaining a sufficient number of modes in Galerkin discretisation. The frequency-amplitude diagrams for all generalised coordinates are depicted in Fig. 7. As seen, the 6-DOF model employed in this study ensure converged results; it is seen that the amplitude of sixth generalised coordinate is very small compared to that of the first generalised coordinate indicating convergence. The phase-plane plots and time histories of w, θ, and u are shown in Figs. 8 and 9 for excitation frequencies ω_b=1.9877 ω_1 and ω_b=2.0704 ω_1, respectively. The time history of the transverse motion in Fig. 9 clearly shows that the transverse motion reaches its maximum amplitude before the tip angle reaching its maximum.

The effect of the axial base excitation amplitude on the transverse motion parametric resonance response is shown in Fig. 10; the oscillation envelope is plotted in this figure by plotting both maximum and minimum transverse displacements. As seen, the whole parametric resonance region becomes wider with increasing base excitation amplitude. Additionally, at sufficiently large base excitation amplitudes, the tip transverse displacement corresponding to maximum tip rotation reaches a local maximum and then decreases.

The effect of the added tip mass ratio γ on nonlinear frequency-amplitude responses of the system is depicted in Fig. 11. As seen, increasing the added tip mass ratio results in parametric resonance region shifting to the left on the frequency axis, which is an indication of reduced natural frequency. As seen in sub-figure (b), the tip axial displacement magnitude increases slightly with increasing tip mass ratio.

4.2 Parametric resonance due to varying base excitation amplitude

Parametric resonance could occur when the amplitude of the axial base excitation is changed as the bifurcation parameter given that the base-excitation frequency is set to a value near twice the fundamental natural frequency. An example of that is shown in Fig. 12 when ω_b is set to 2.00 ω_1 and x_b is varied as the control parameter. It is interesting to note that a period-doubling bifurcation occurs at point P, corresponding to x_b= 0.0043, which renders the trivial configuration unstable and results in bifurcation of a nontrivial stable solution branch. It is worth mentioning that for any base excitation amplitude less than 0.0043, parametric resonance does not occur in the cantilever. Hence, based on the assumed material viscosity of 0.004, a minimum axial base excitation amplitude of x_b=0.0043 is required for the occurrence of parametric resonance. To gain a better understanding of this minimum required value for parametric resonance, it is interesting to compare the dimensionless load in the dynamic case to the dimensionless self-weight buckling load. Conducting a static self-weight buckling analysis reveals that buckling occurs at a dimensionless load of $\chi = \rho A L^3 g/(EI) = 7.8375$, which is in agreement with the values reported in the literature. Knowing that parametric resonance occurs when x_b=0.0043 and ω_b=2.00ω_1, with ω_1=3.5160, the minimum dimensionless load corresponding to parametric

resonance is obtained as $x_b\omega_b^2$ = 0.2126, which is almost 2.7% of the self-weight buckling load.

The tip transverse displacement corresponding to maximum tip rotation for two base excitation frequencies of 2.05 ω_1 and 2.10 ω_1 are shown in Fig. 13 (a, b), respectively. As seen, for both cases, after the occurrence of the period-doubling bifurcation at point P, an unstable nontrivial solution is bifurcated from the original trivial branch. This unstable branch regains stability via a saddle-node bifurcation; for the case with ω_b =2.10 ω_1, two more saddle-node bifurcations appear with increasing base excitation amplitude.

The tip mass ratio effect on parametric resonance of the cantilever is illustrated in Fig. 14. The frequency of the base excitation is set to 7.10 for all cases. As seen, increasing the tip mass ratio postpones the nontrivial solution bifurcation to larger base excitation amplitudes. Additionally, for larger tip mass ratios, the cantilever shows more complex parametric resonance response with three saddle-node bifurcations.

5. Conclusions

The nonlinear parametric resonance response of a cantilever under axial base excitation is examined via developing a geometrically exact model capable of capturing extremely large oscillation amplitudes accurately. The Euler-Bernoulli beam theory along with centreline inextensibility is utilised to derive the equation of motion for centreline rotation, while employing the Kelvin-Voigt model to model internal energy dissipation. Galerkin's technique is utilised to obtain the discretised set of equations which are then solved using a continuation technique.

A comparison of the developed model to a three-dimensional nonlinear finite element model showed that it can capture extremely large deformations accurately.

Examining the nonlinear parametric resonance of the cantilever when the frequency of the axial base excitation is varied as the bifurcation parameter showed that the oscillation amplitude grows very large after the occurrence of the period-doubling bifurcations. Tracking the tip transverse amplitude corresponding to maximum tip rotation revealed that it reaches a maximum and then decreases with increasing frequency. It is shown that the addition of a tip mass shifts the parametric resonance region to smaller excitation frequencies.

It was shown that when the amplitude of the base excitation is changed as the bifurcation parameter, no parametric resonance occurs for excitation amplitudes smaller than 0.0043; it was shown that this base excitation amplitude is equivalent to a dimensionless dynamic load amplitude of 0.2126, which is almost 2.7% of the self-weight buckling load. Additionally, depending on the excitation frequency, the parametric

resonance region consists of zero, one, or three saddle-node bifurcations. For a fixed excitation frequency, it was shown that the addition of a tip mass postpones the occurrence of the period-doubling bifurcation to larger amplitudes of the base excitation.

Appendix A. The significance of a geometrically exact model

In this appendix, the static and dynamic responses of a cantilever are examined using the proposed exact model for centreline rotation and a third-order nonlinear model for the transverse motion. The third-order model accounts for geometric and inertial nonlinearities and utilises a Kelvin-Voigt damping mechanism for the purpose of consistency with the proposed model for the dynamic analysis. The comparison of the two models is shown in Fig. 15. Sub-figure (a) shows the comparison between the two models in predicting the static response of a cantilever with a tip load in the z direction; f_0 denotes the nondimensional load ($f_0 = fL^2/(EI)$). As seen, third-order model deviates from the exact model at tip static deflection of around 40% of the length, occurring in the vicinity of f_0=1.2; beyond that, the third-order model error increases rapidly.

Figure 15(b) shows the comparison between the parametric resonance responses of the cantilever using the two models when ω_b/ω_1=2.0. As seen, both models predict almost the same base excitation amplitude for the occurrence of the period-doubling bifurcation. However, beyond that point, the third-order model loses accuracy very rapidly with increasing base excitation amplitude. The differences between the two models for both static and dynamic cases clearly signify the importance of employing a geometrically exact model based on rotation when examining the large-amplitude response of cantilevers.

References

[1] M. Javani, Y. Kiani, M.R. Eslami, Free vibration of arbitrary thick FGM deep arches using unconstrained higher-order shear deformation theory, Thin-Walled Structures, 136 (2019) 258-266.
[2] H. Tang, L. Li, Y. Hu, W. Meng, K. Duan, Vibration of nonlocal strain gradient beams incorporating Poisson's ratio and thickness effects, Thin-Walled Structures, 137 (2019) 377-391.
[3] Z.J. Zhang, Q.C. Zhang, F.C. Li, J.W. Yang, J.W. Liu, Z.Y. Liu, F. Jin, Modal characteristics of micro-perforated sandwich beams with square honeycomb-corrugation hybrid cores: A mixed experimental-numerical study, Thin-Walled Structures, 137 (2019) 185-196.
[4] S. Zheng, D. Chen, H. Wang, Size dependent nonlinear free vibration of axially functionally graded tapered microbeams using finite element method, Thin-Walled Structures, 139 (2019) 46-52.
[5] H. Babaei, Y. Kiani, M.R. Eslami, Geometrically nonlinear analysis of functionally graded shallow curved tubes in thermal environment, Thin-Walled Structures, 132 (2018) 48-57.
[6] A. Ghorbani Shenas, S. Ziaee, P. Malekzadeh, Nonlinear vibration analysis of pre-twisted functionally graded microbeams in thermal environment, Thin-Walled Structures, 118 (2017) 87-104.
[7] O.G. McGee, Closed-form effects of warping and pretwist on the torsional vibration of thin-walled open-profile cantilevers, Thin-Walled Structures, 13 (1992) 217-244.
[8] Z.c. Qiu, H.x. Wu, D. Zhang, Experimental researches on sliding mode active vibration control of flexible piezoelectric cantilever plate integrated gyroscope, Thin-Walled Structures, 47 (2009) 836-846.
[9] V. Kumar, J.W. Boley, Y. Yang, H. Ekowaluyo, J.K. Miller, G.T.-C. Chiu, J.F. Rhoads, Bifurcation-based mass sensing using piezoelectrically-actuated microcantilevers, Applied Physics Letters, 98 (2011) 153510.
[10] S.N. Mahmoodi, N. Jalili, Non-linear vibrations and frequency response analysis of piezoelectrically driven microcantilevers, International Journal of Non-Linear Mechanics, 42 (2007) 577-587.
[11] M.I. Friswell, S.F. Ali, O. Bilgen, S. Adhikari, A.W. Lees, G. Litak, Non-linear piezoelectric vibration energy harvesting from a vertical cantilever beam with tip mass, Journal of Intelligent Material Systems and Structures, 23 (2012) 1505-1521.
[12] H. Liu, C. Lee, T. Kobayashi, C.J. Tay, C. Quan, Piezoelectric MEMS-based wideband energy harvesting systems using a frequency-up-conversion cantilever stopper, Sensors and Actuators A: Physical, 186 (2012) 242-248.
[13] M. Crespo da Silva, C. Glynn, Nonlinear flexural-flexural-torsional dynamics of inextensional beams. I. Equations of motion, Journal of Structural Mechanics, 6 (1978) 437-448.
[14] M. Crespo da Silva, C. Glynn, Nonlinear flexural-flexural-torsional dynamics of inextensional beams. II. Forced motions, Journal of Structural Mechanics, 6 (1978) 449-461.
[15] A.H. Nayfeh, P.F. Pai, Non-linear non-planar parametric responses of an inextensional beam, International Journal of Non-Linear Mechanics, 24 (1989) 139-158.
[16] P.F. Pai, A.H. Nayfeh, Non-linear non-planar oscillations of a cantilever beam under lateral base excitations, International Journal of Non-Linear Mechanics, 25 (1990) 455-474.
[17] Z. Feng, L. Leal, Symmetries of the amplitude equations of an inextensional beam with internal resonance, Journal of applied mechanics, 62 (1995) 235-238.
[18] T. Anderson, A. Nayfeh, B. Balachandran, Experimental verification of the importance of the nonlinear curvature in the response of a cantilever beam, Journal of Vibration and Acoustics, 118 (1996) 21-27.
[19] M. Hamdan, M. Dado, Large amplitude free vibrations of a uniform cantilever beam carrying an intermediate lumped mass and rotary inertia, Journal of Sound and Vibration, 206 (1997) 151-168.
[20] H.N. Arafat, A.H. Nayfeh, C.-M. Chin, Nonlinear nonplanar dynamics of parametrically excited cantilever beams, Nonlinear Dynamics, 15 (1998) 31-61.
[21] E. Esmailzadeh, N. Jalili, Parametric response of cantilever Timoshenko beams with tip mass under harmonic support motion, International Journal of Non-Linear Mechanics, 33 (1998) 765-781.

[22] H. Farokhi, M.H. Ghayesh, S. Hussain, Large-amplitude dynamical behaviour of microcantilevers, International Journal of Engineering Science, 106 (2016) 29-41.
[23] M.-R. Ghazavi, G. Rezazadeh, S. Azizi, Pure parametric excitation of a micro cantilever beam actuated by piezoelectric layers, Applied Mathematical Modelling, 34 (2010) 4196-4207.
[24] S.N. Mahmoodi, N. Jalili, M. Ahmadian, Subharmonics analysis of nonlinear flexural vibrations of piezoelectrically actuated microcantilevers, Nonlinear Dynamics, 59 (2010) 397-409.
[25] S. Leadenham, A. Erturk, Unified nonlinear electroelastic dynamics of a bimorph piezoelectric cantilever for energy harvesting, sensing, and actuation, Nonlinear Dynamics, 79 (2015) 1727-1743.
[26] Y.-Q. Tang, L.-Q. Chen, Stability analysis and numerical confirmation in parametric resonance of axially moving viscoelastic plates with time-dependent speed, European Journal of Mechanics-A/Solids, 37 (2013) 106-121.
[27] L.-Q. Chen, Y.-Q. Tang, J.W. Zu, Nonlinear transverse vibration of axially accelerating strings with exact internal resonances and longitudinally varying tensions, Nonlinear Dynamics, 76 (2014) 1443-1468.
[28] Y.-Q. Tang, D.-B. Zhang, J.-M. Gao, Parametric and internal resonance of axially accelerating viscoelastic beams with the recognition of longitudinally varying tensions, Nonlinear Dynamics, 83 (2016) 401-418.

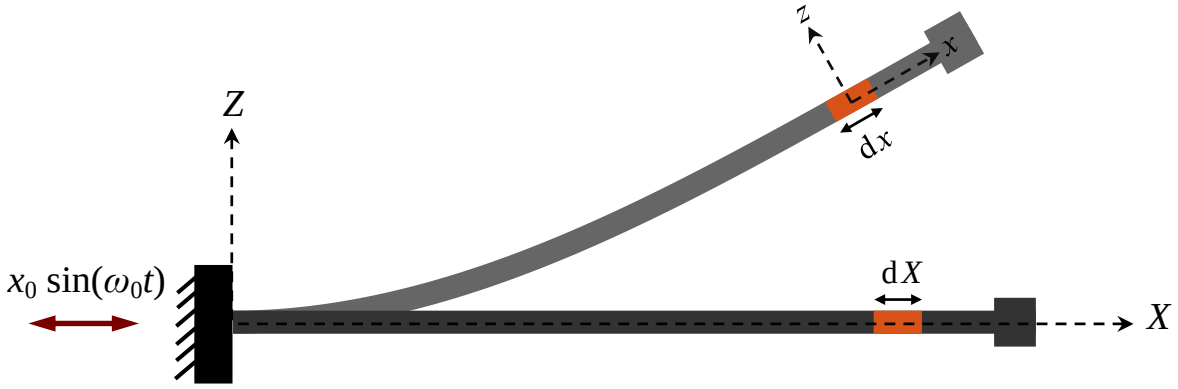

Fig. 1. Schematic illustration of a cantilever with a tip mass under axial base excitation.

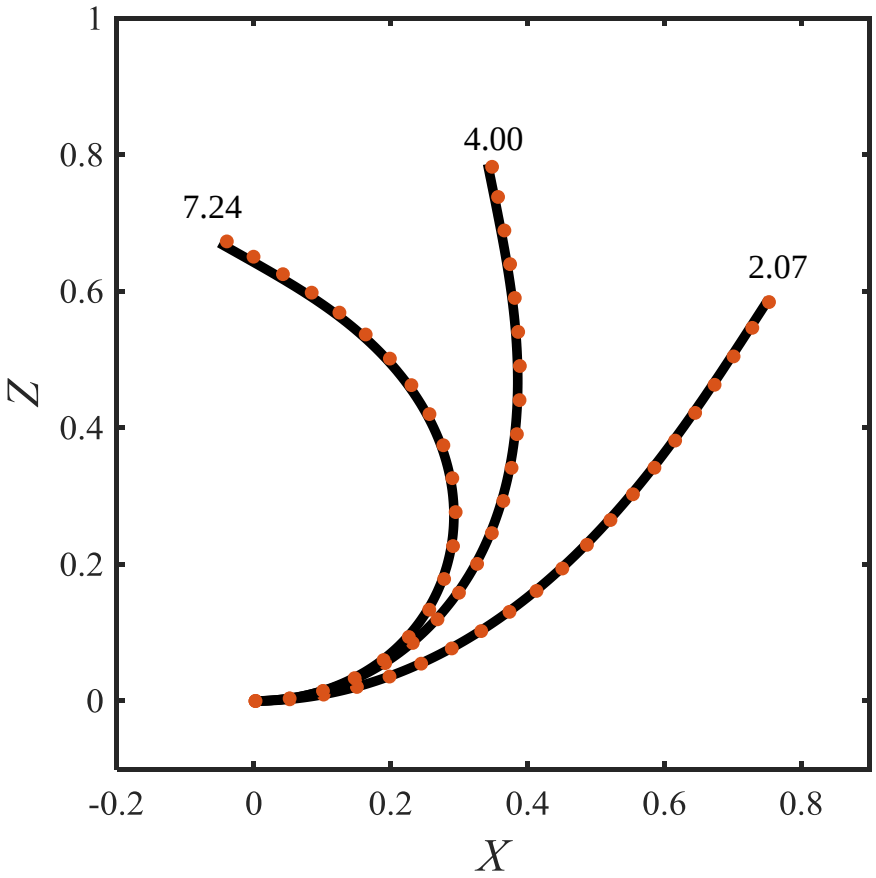

Fig.2. Nonlinear static deformation of the cantilever at different force levels (shown on the curves). Solid line and symbols denote the results obtained by the model developed in this study and those obtained via the 3D nonlinear FEA, respectively. *X* and *Z* are dimensionless relative to the length.

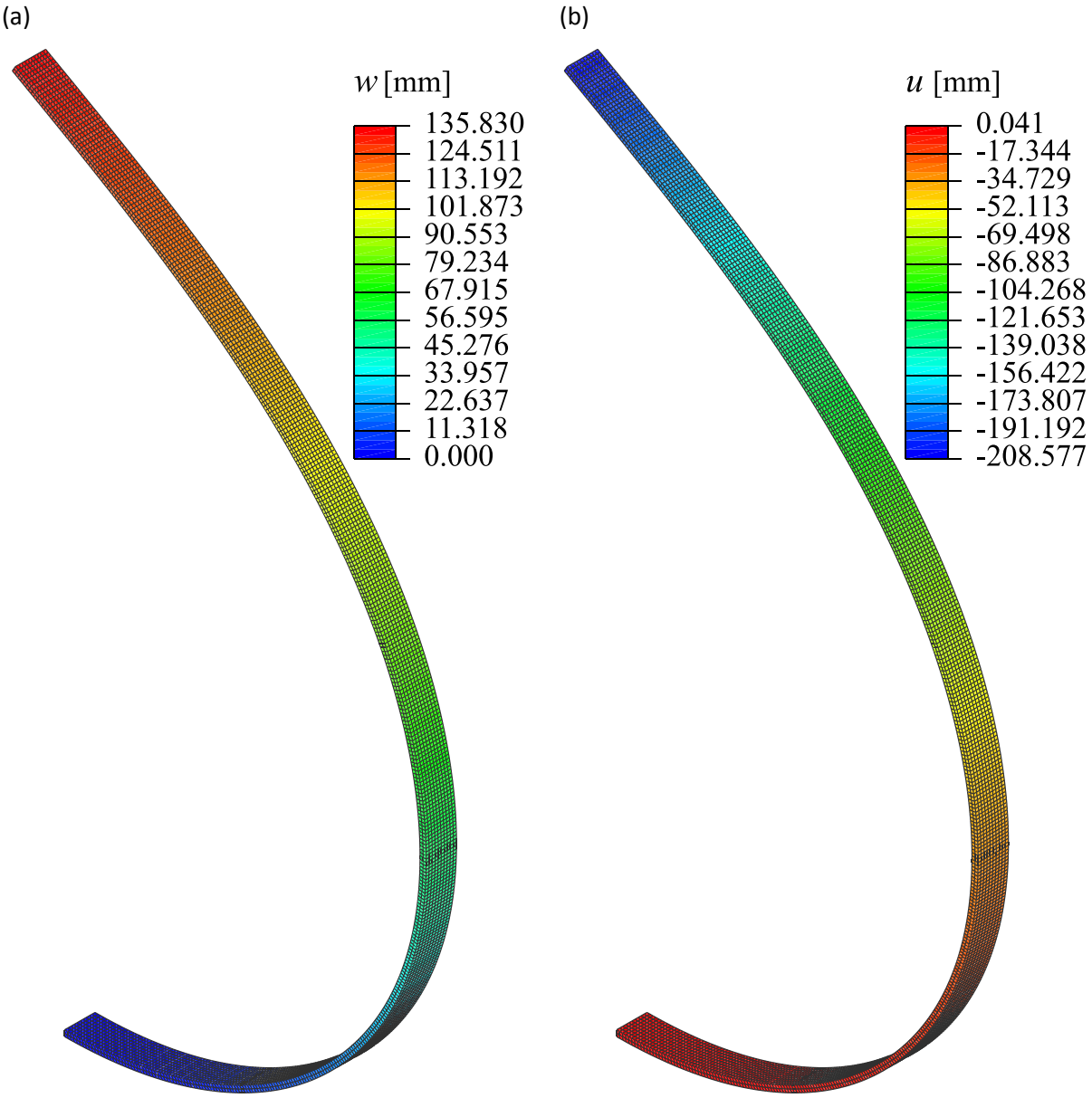

Fig. 3. 3D nonlinear FEA contour plots of (a) transverse and (b) axial static deformations of the cantilever of Fig. 2 for the case F_{tip}=7.24.

(a)

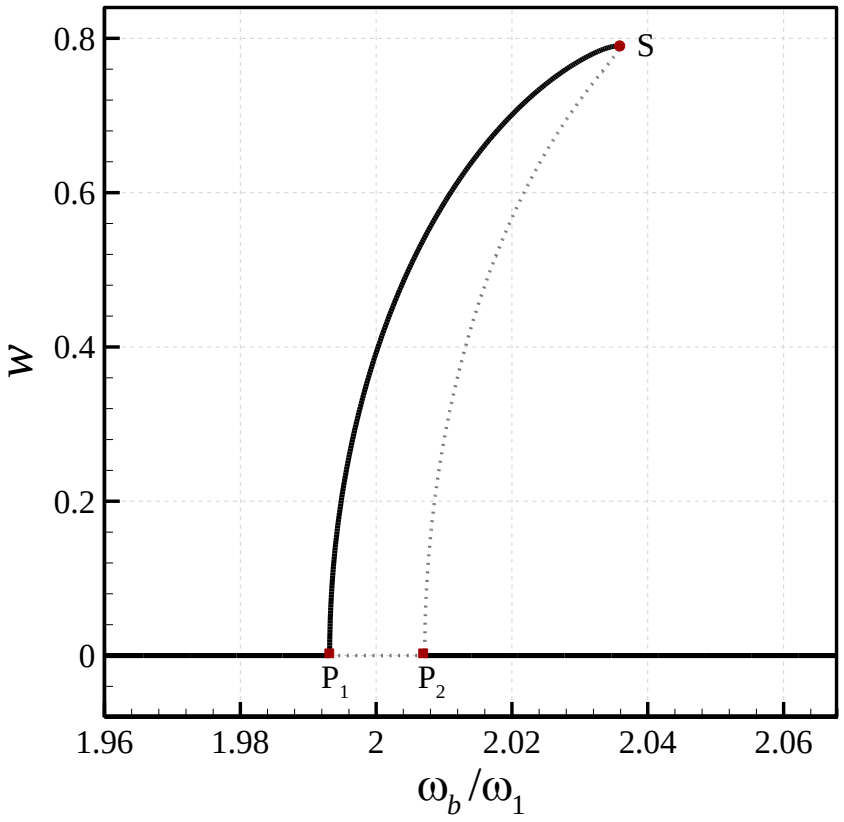
0.8
0.6
0.4
0.2
0
w
S
P1
P2
1.96
1.98
2
2.02
2.04
2.06
ωb/ω1

(b)

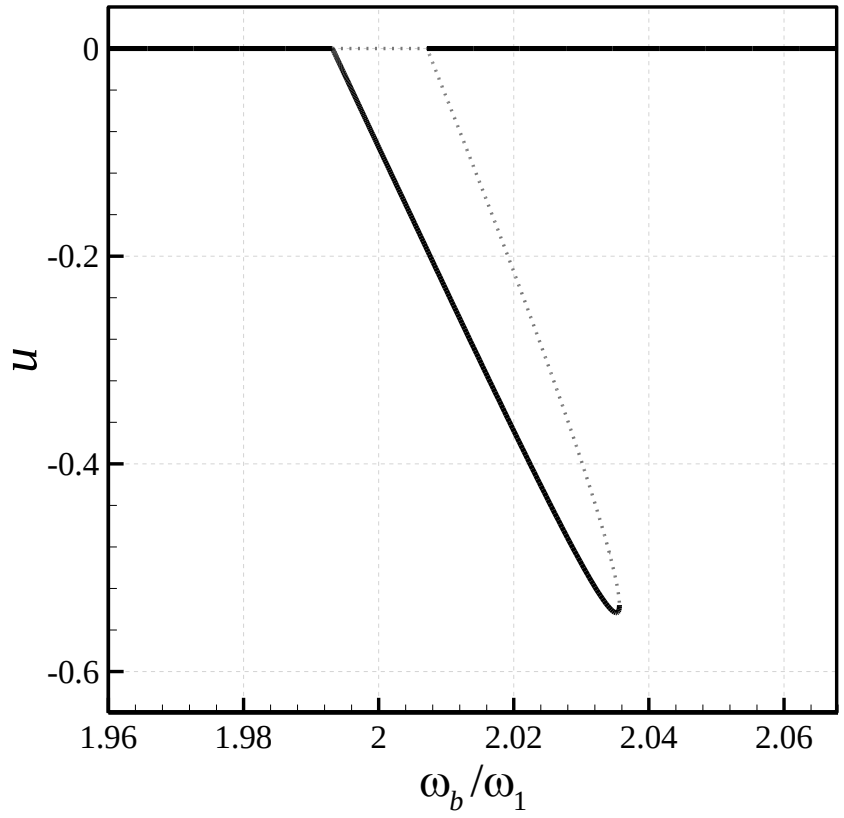
0
-0.2
-0.4
-0.6
u
1.96
1.98
2
2.02
2.04
2.06
ωb/ω1

(c)

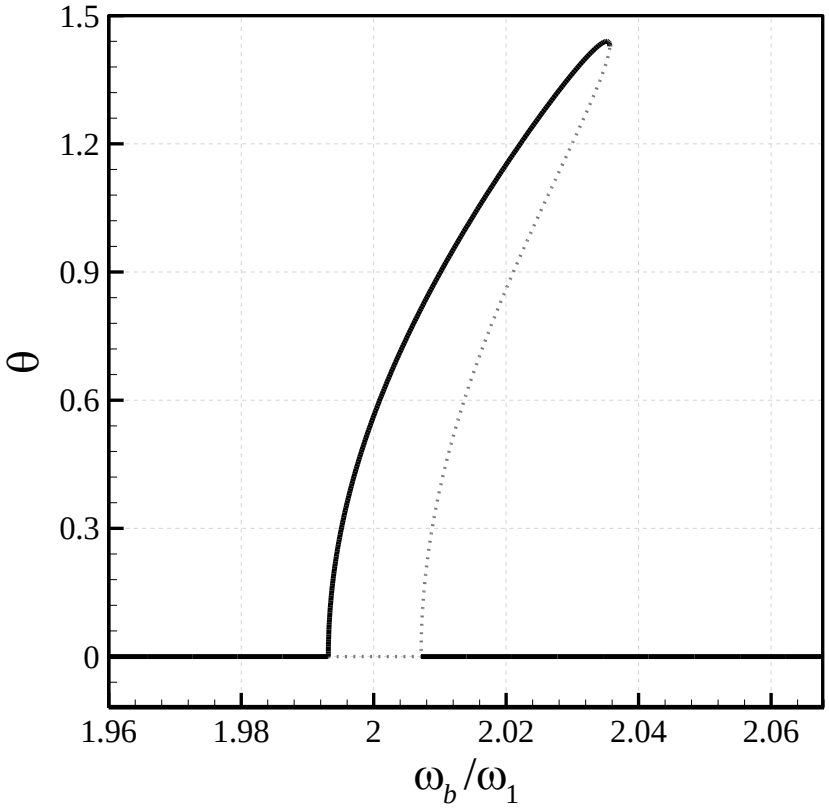

Fig.4. Parametric resonance of the cantilever under axial base excitation; (a, b) transverse and axial tip displacements, respectively, corresponding to maximum tip rotation (c). x_b=0.005, γ=0, and ω_1=3.5160.

(a)

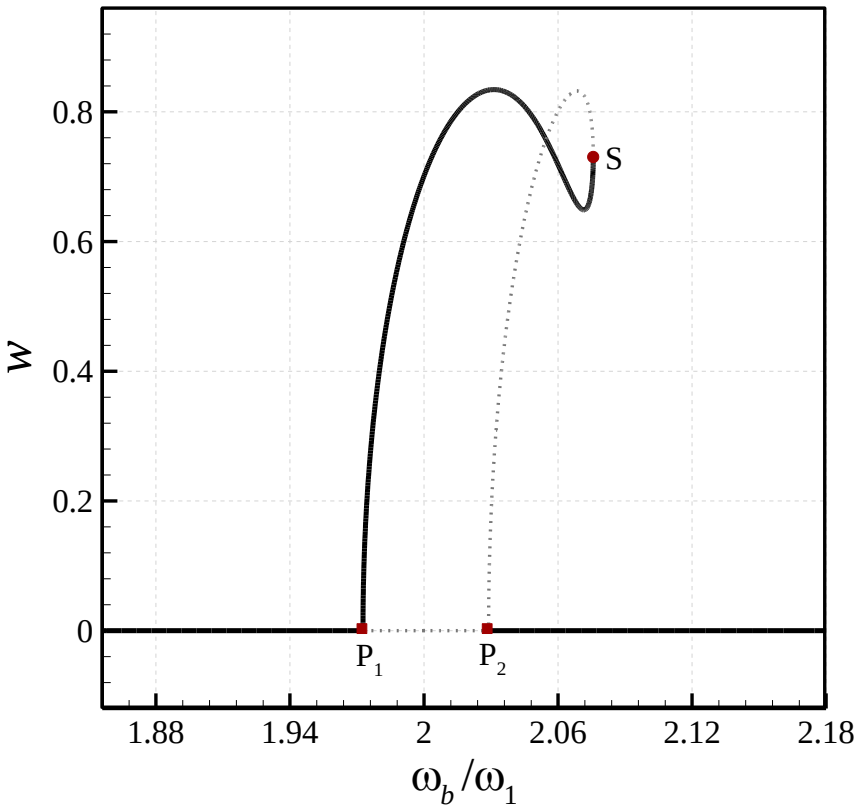
0.8
0.6
0.4
0.2
0
w
S
P1
P2
1.88
1.94
2
2.06
2.12
2.18
ωb/ω1

(b)

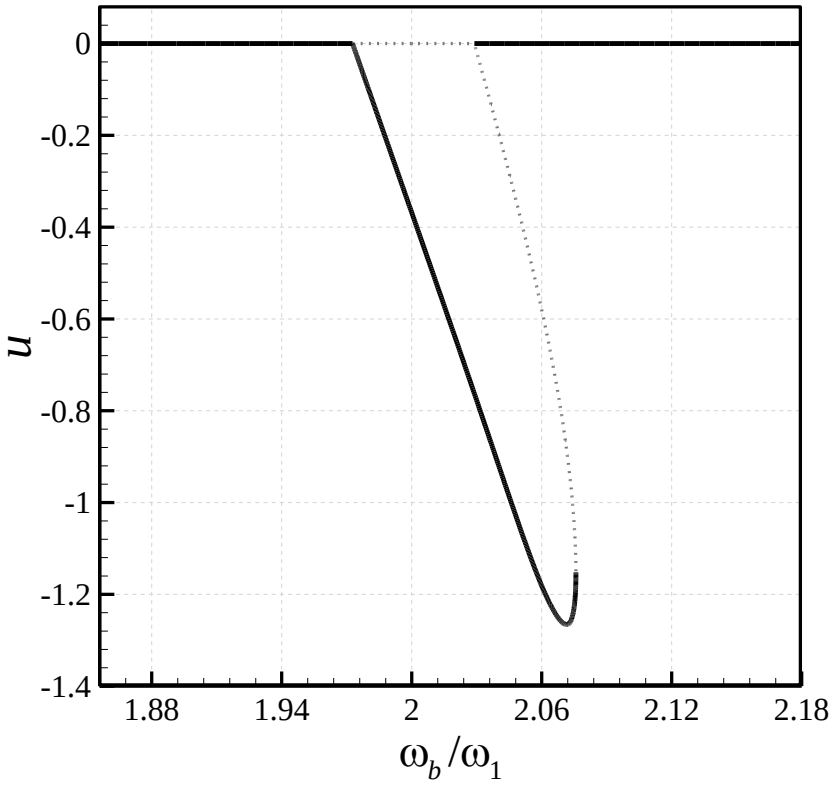
0
-0.2
-0.4
-0.6
-0.8
-1
-1.2
-1.4
u
1.88
1.94
2
2.06
2.12
2.18
ωb/ω1

(c)

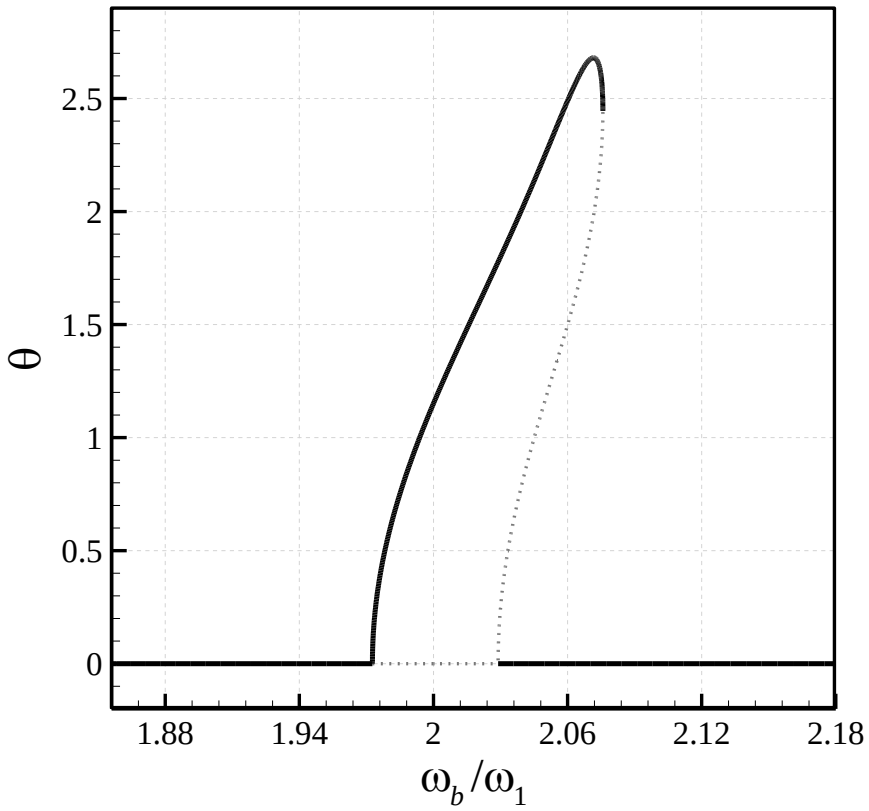

Fig.5. Parametric resonance of the cantilever under axial base excitation; (a, b) transverse and axial tip displacements, respectively, corresponding to maximum tip rotation (c). x_b=0.01, γ=0, and ω_1=3.5160.

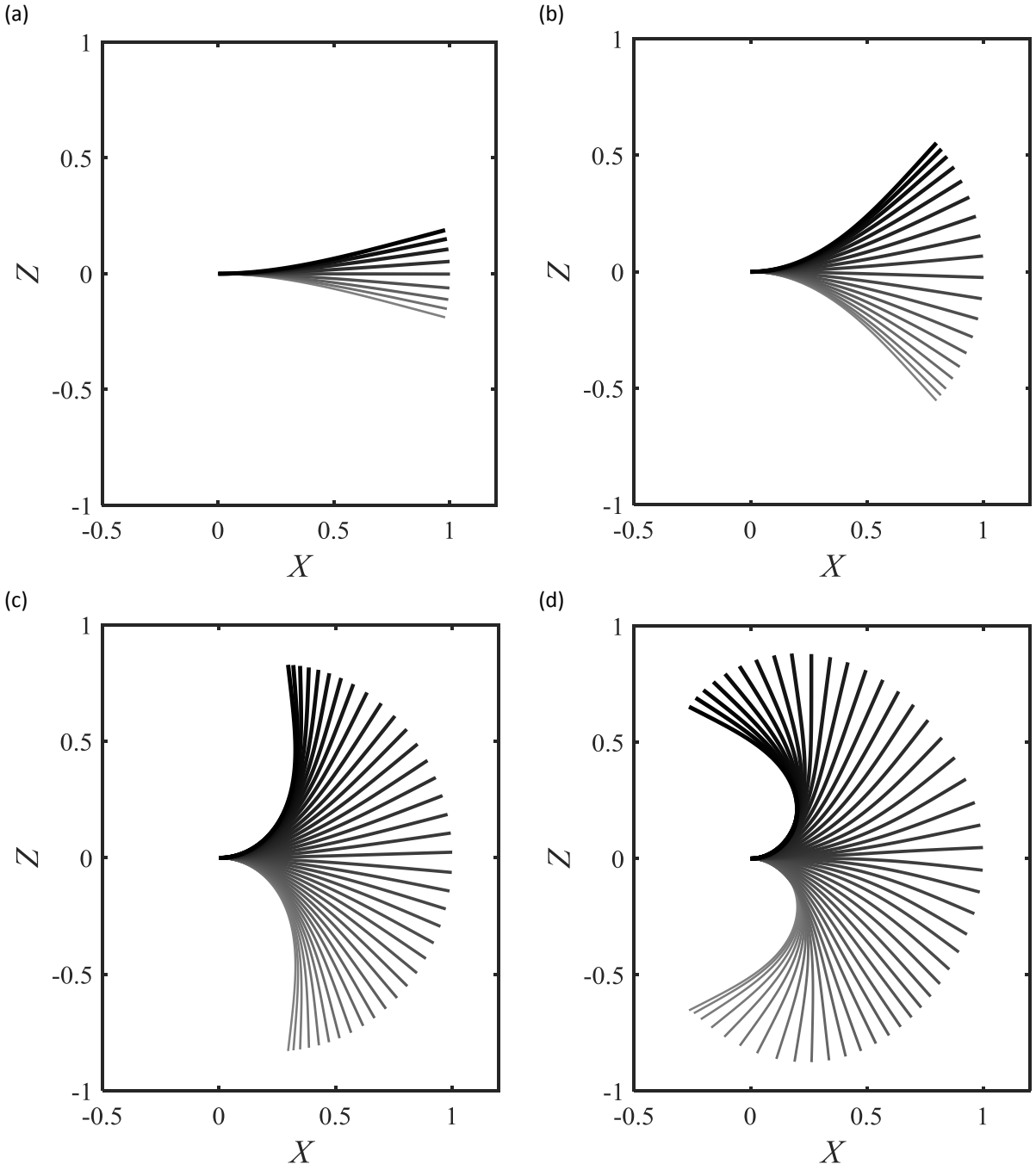

Fig.6. Oscillation of the system of Fig. 5 at (a) ω_b/ω_1=1.9742, (b) ω_b/ω_1=1.9877, (c) ω_b/ω_1=2.0247, and (d) ω_b/ω_1=2.0704. *X* and *Z* are dimensionless relative to the length.

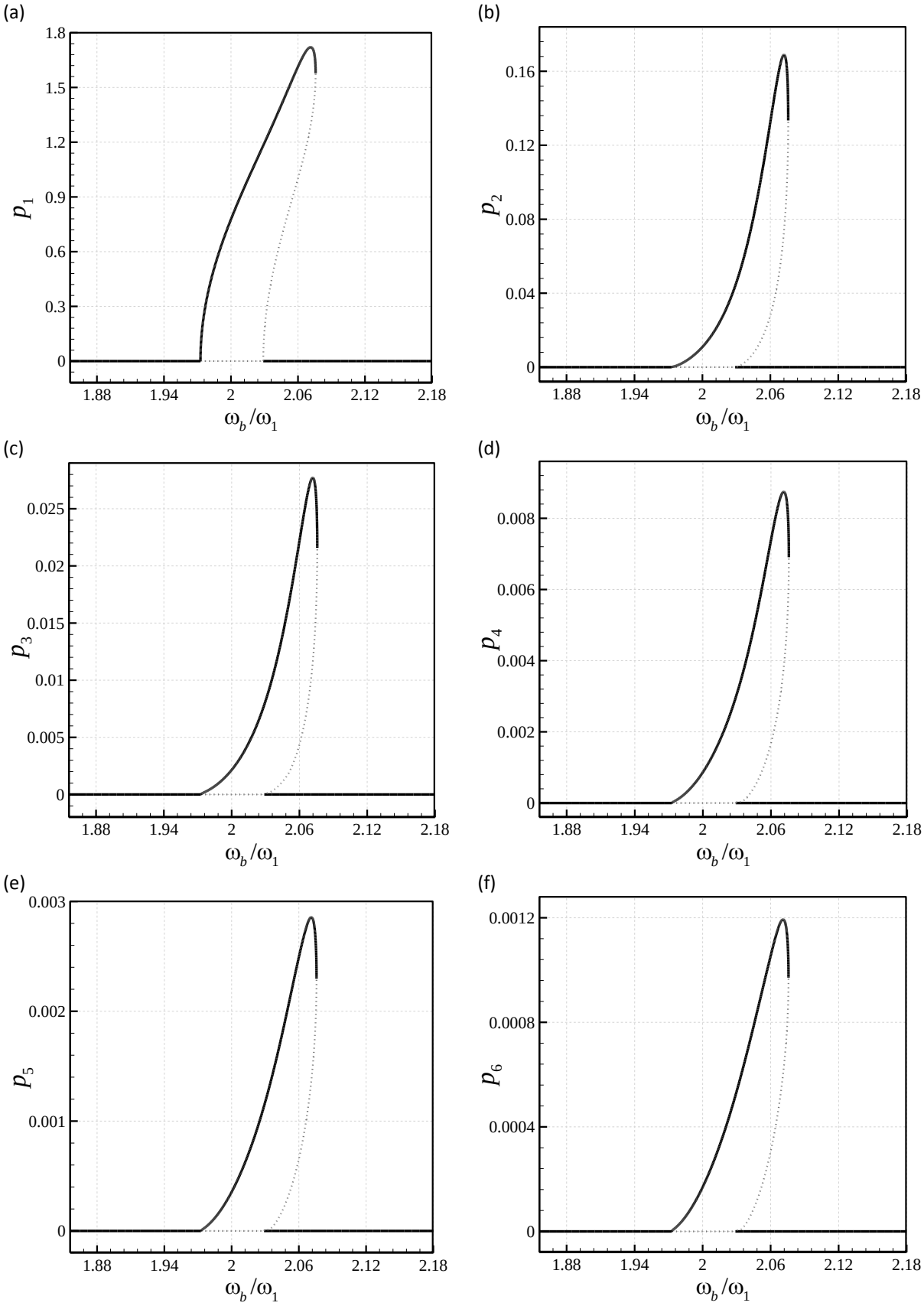

Fig.7. Rotational motion generalised coordinates of the system of Fig. 5.

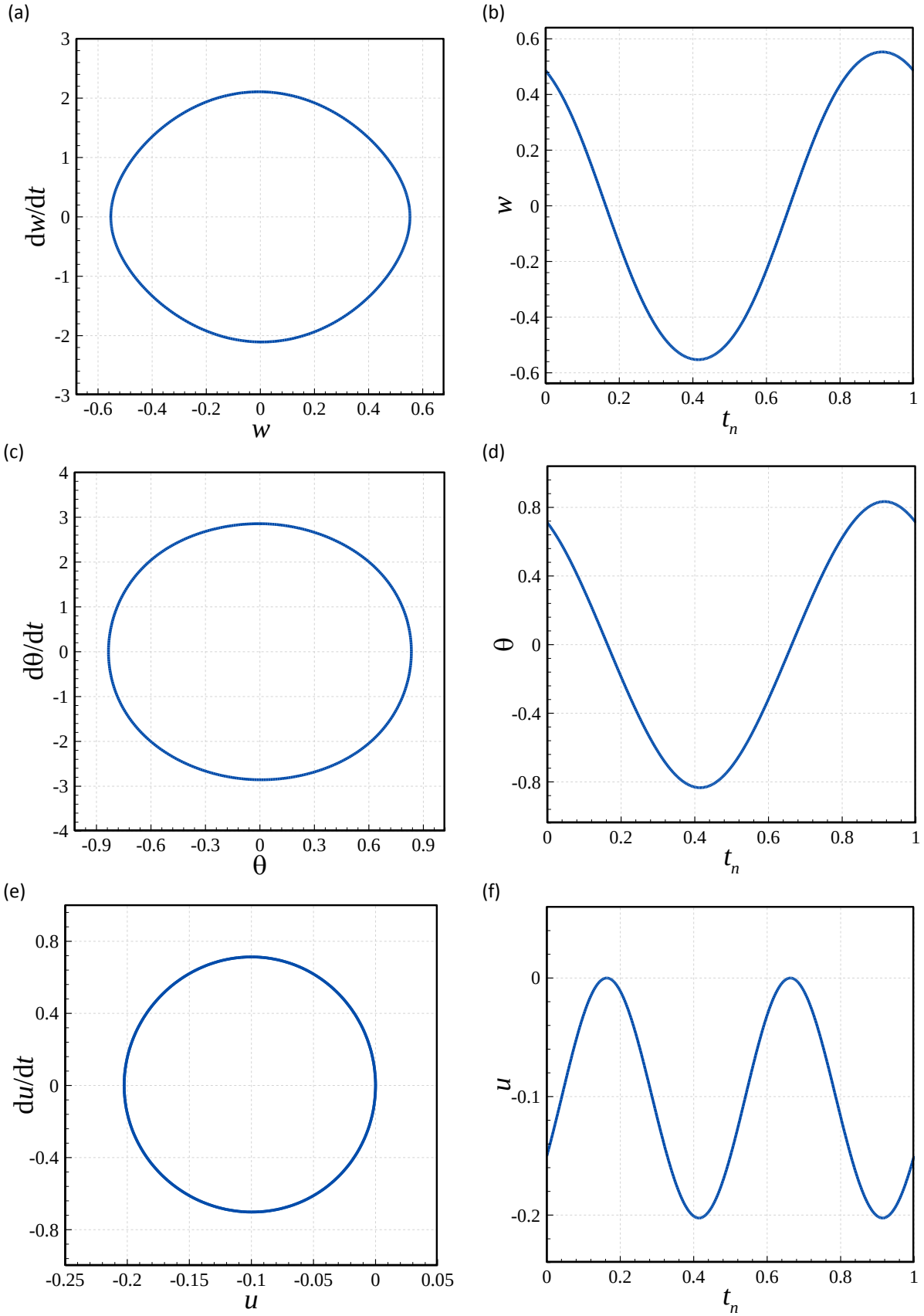

Fig.8. Dynamics of the system of Fig. 5 at ω_b/ω_1=1.9877. Phase-plane plots and time histories of (a, b) *w* at tip, (c, d) θ at tip, and (e, f) *u* at tip. t_n : normalised time relative to the oscillation period.

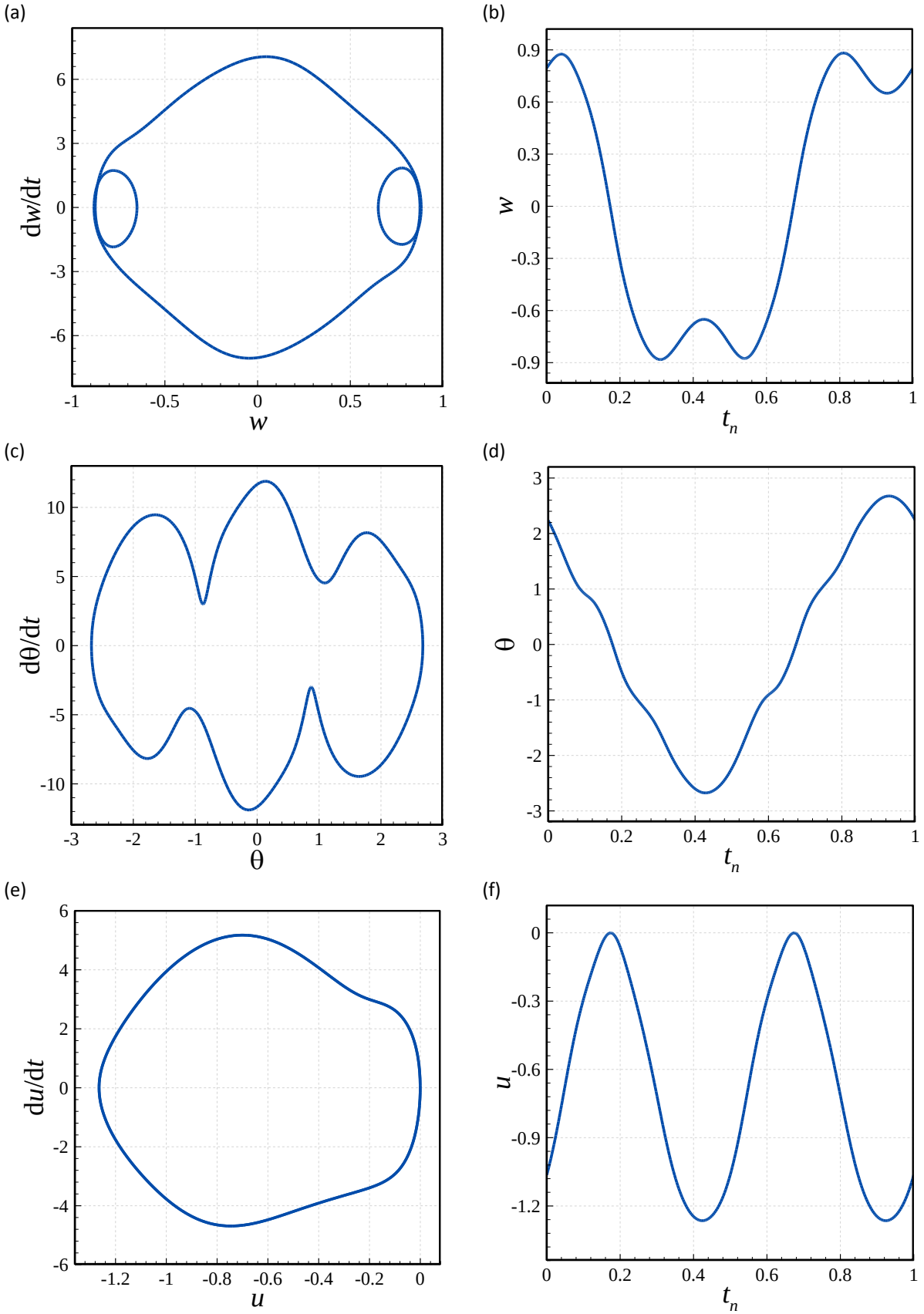

Fig.9. Dynamics of the system of Fig. 5 at ω_b/ω_1=2.0704. Phase-plane plots and time histories of (a, b) *w* at tip, (c, d) θ at tip, and (e, f) *u* at tip. t_n : normalised time relative to oscillation period.

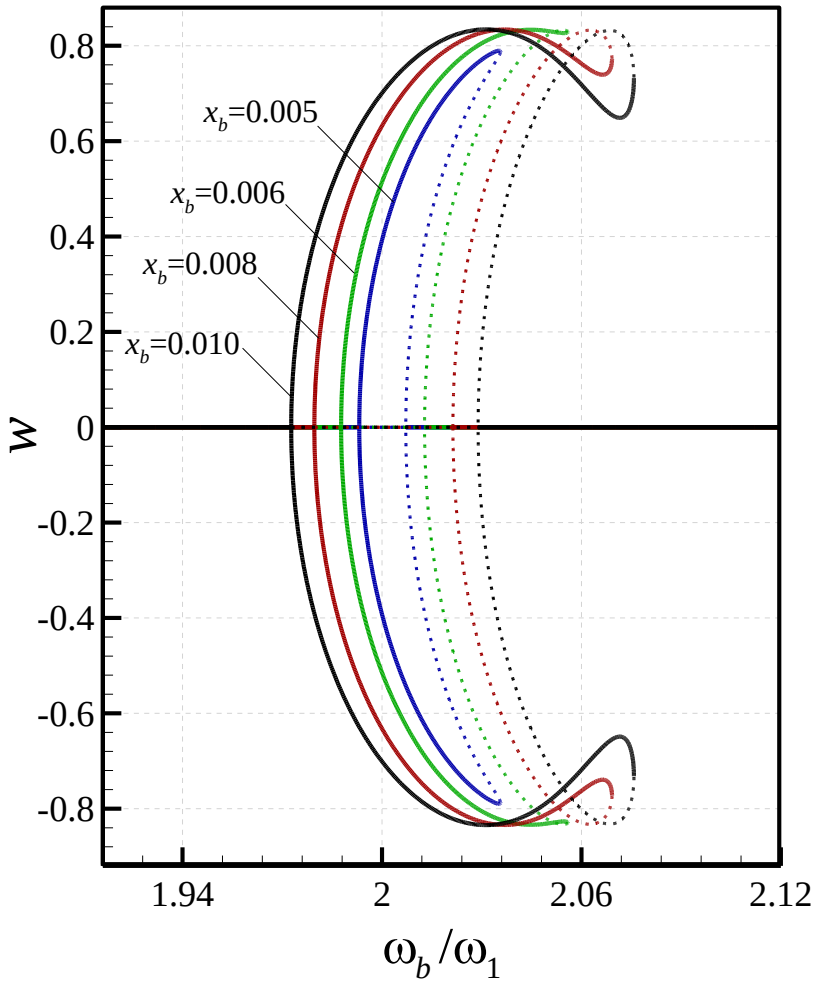

Fig.10. Transverse oscillation envelope of the tip of the cantilever corresponding to maximum tip rotation in parametric resonance for various axial base excitation amplitudes. γ=0 and ω_1=3.5160.

(a)

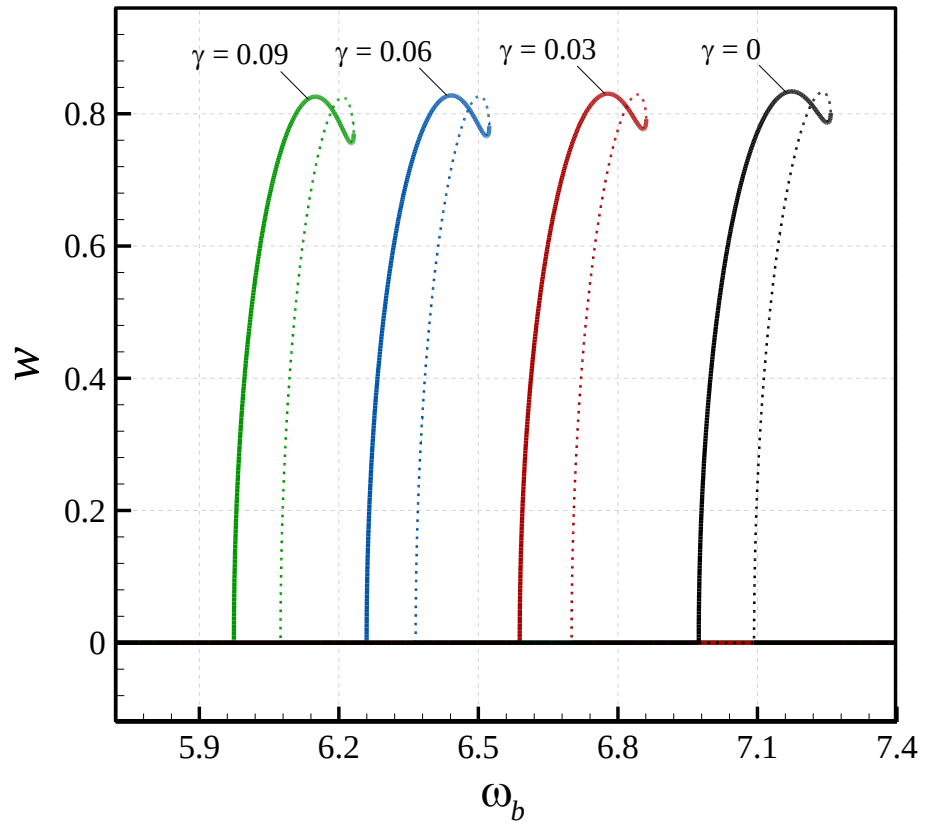

(b)

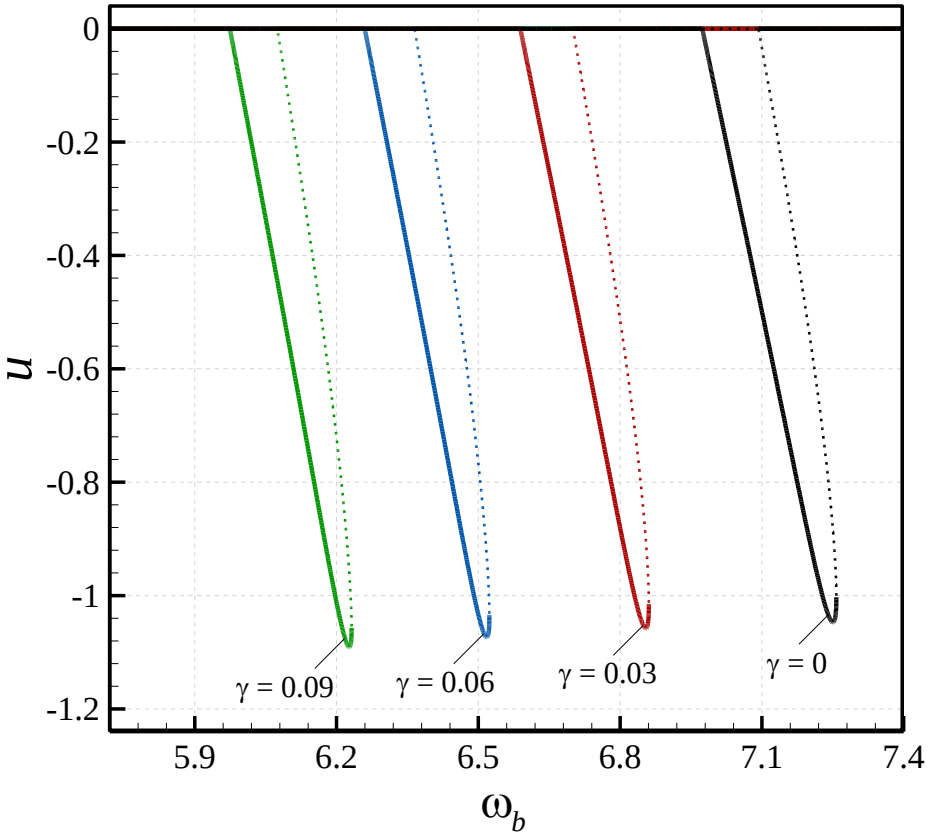

Fig.11. Effect of added tip mass on parametric resonance of the cantilever under axial base excitation; (a,b) tip transverse and axial displacements, respectively, corresponding to maximum tip rotation. x_b=0.007.

(a)

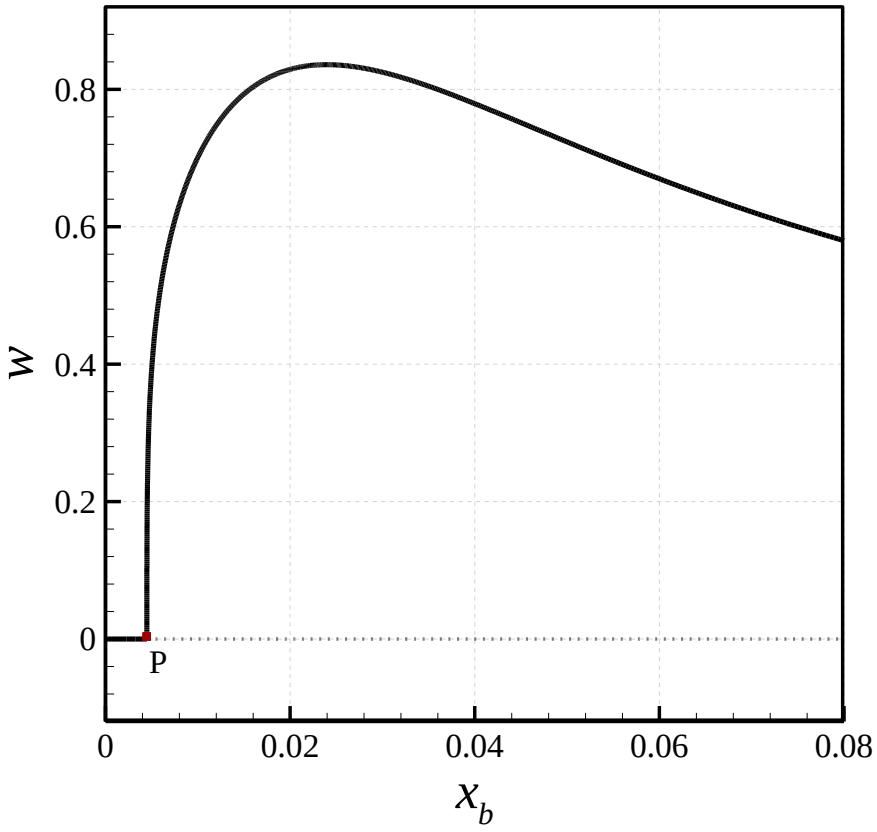
0.8
0.6
0.4
0.2
0
w
P
0
0.02
0.04
0.06
0.08
x_b

(b)

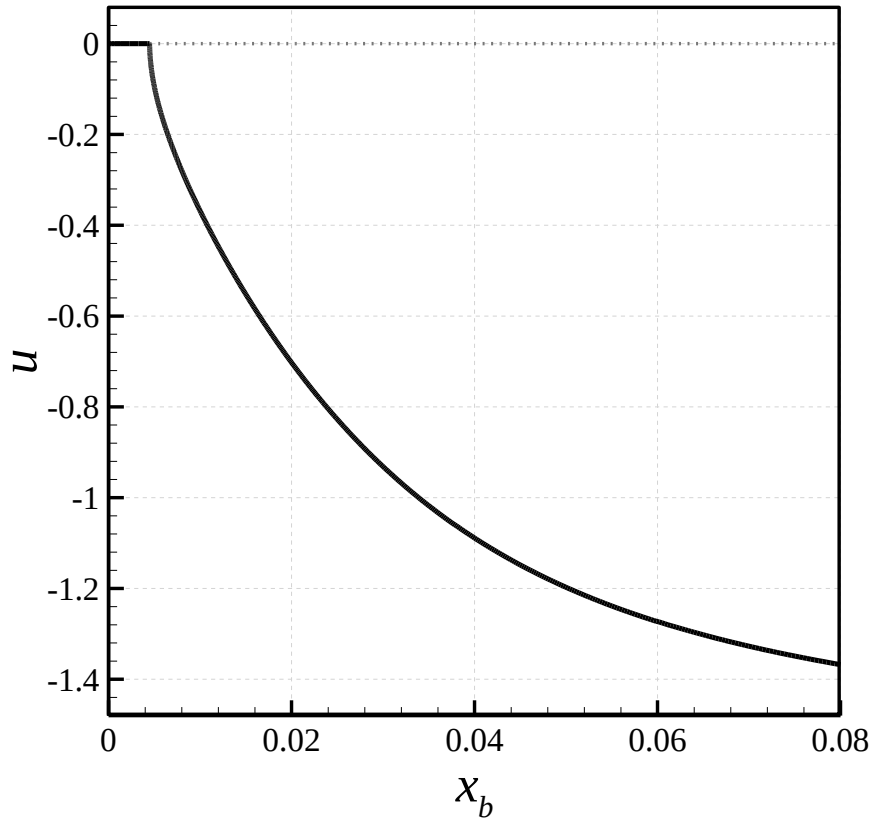
0
-0.2
-0.4
-0.6
-0.8
-1
-1.2
-1.4
u
0
0.02
0.04
0.06
0.08
x_b

(c)

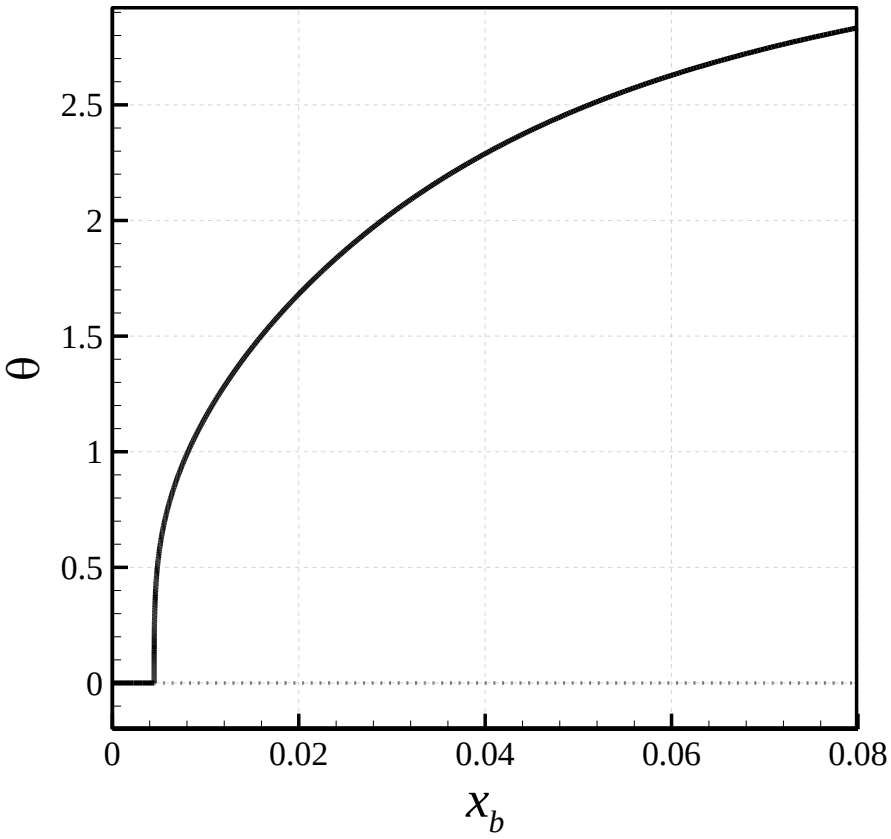

Fig.12. Parametric resonance of the cantilever under axial base excitation; (a, b) transverse and axial tip displacements, respectively, corresponding to maximum tip rotation (c). ω_b/ω_1=2.0.

(a)

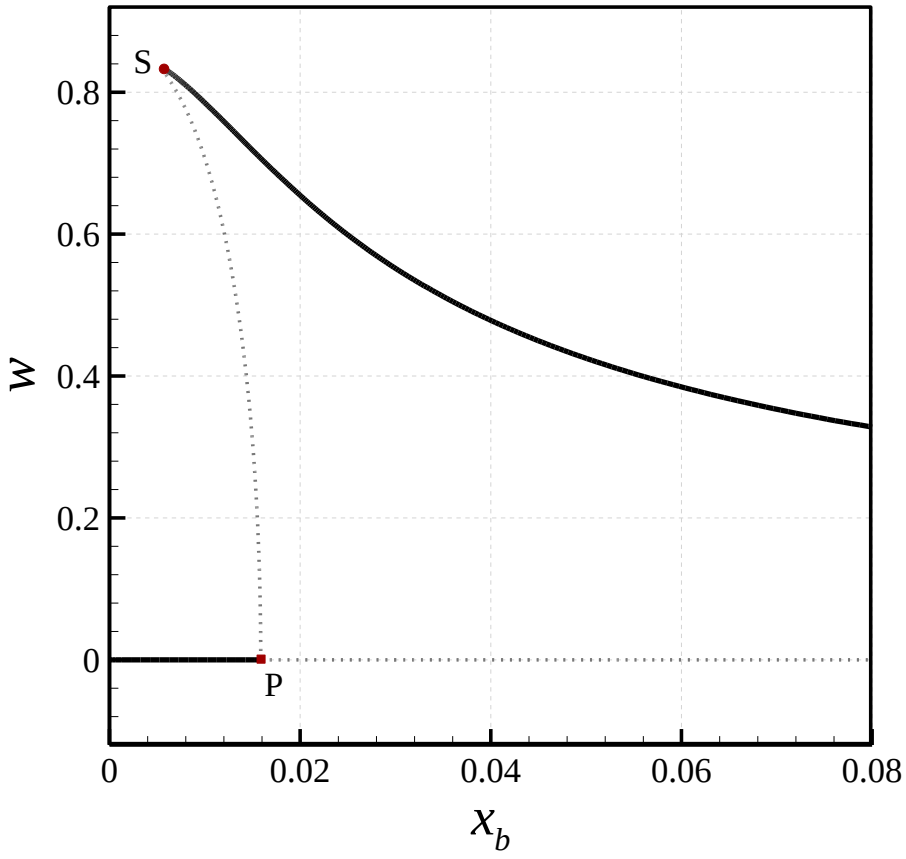

(b)

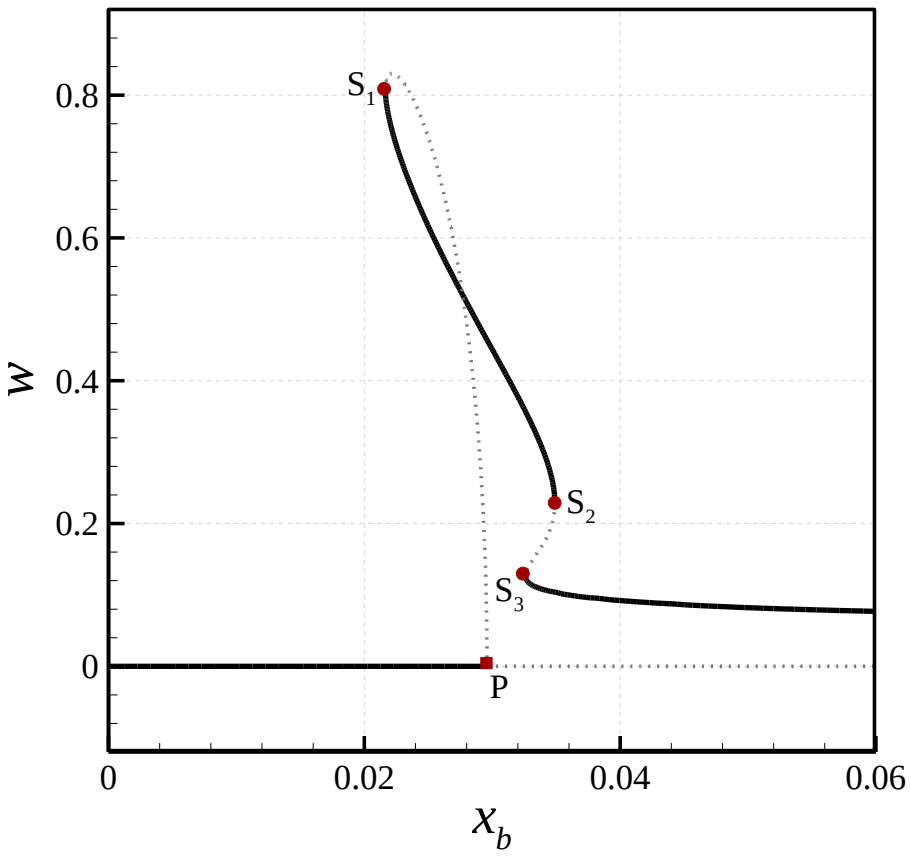

Fig.13. Parametric resonance of the cantilever under axial base excitation; tip transverse motion corresponding to maximum tip rotation when (a) ω_b/ω_1=2.05 and (b) ω_b/ω_1=2.10.

(a)

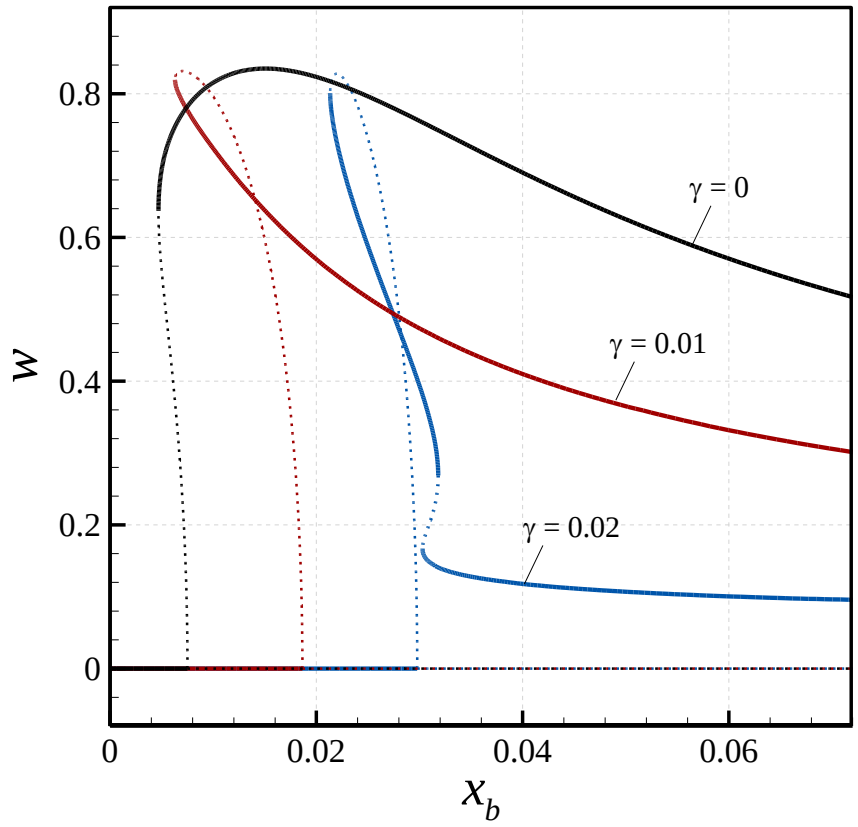

(b)

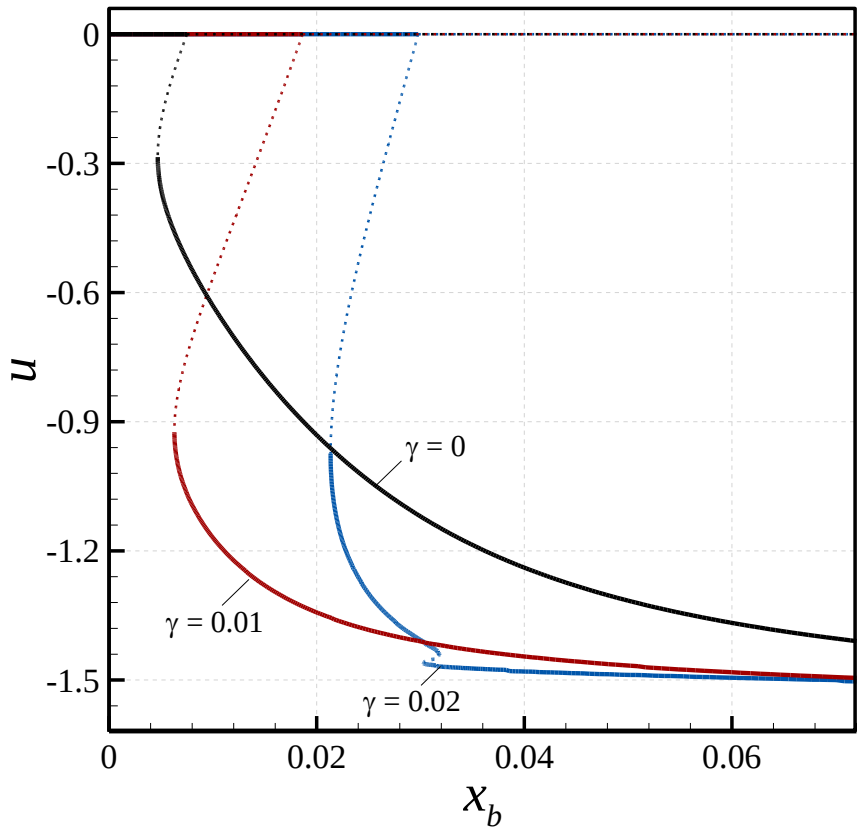

Fig.14. Effect of the added tip mass on parametric resonance of the cantilever under axial base excitation; (a, b) tip transverse and axial displacements, respectively, corresponding to maximum tip rotation. ω_b is set to 7.10 for all cases.

(a)

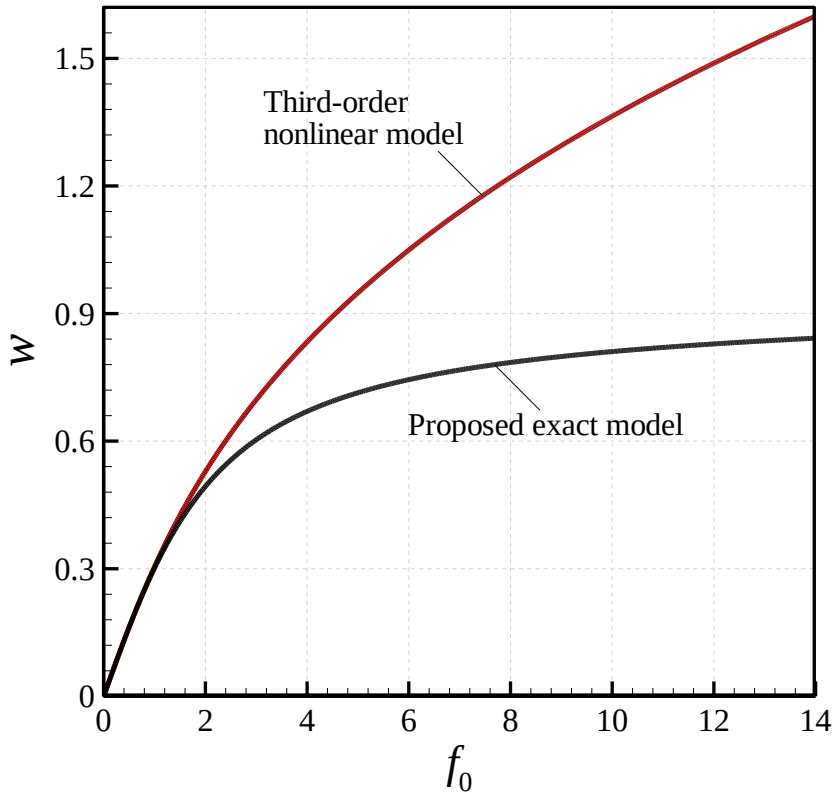

(b)

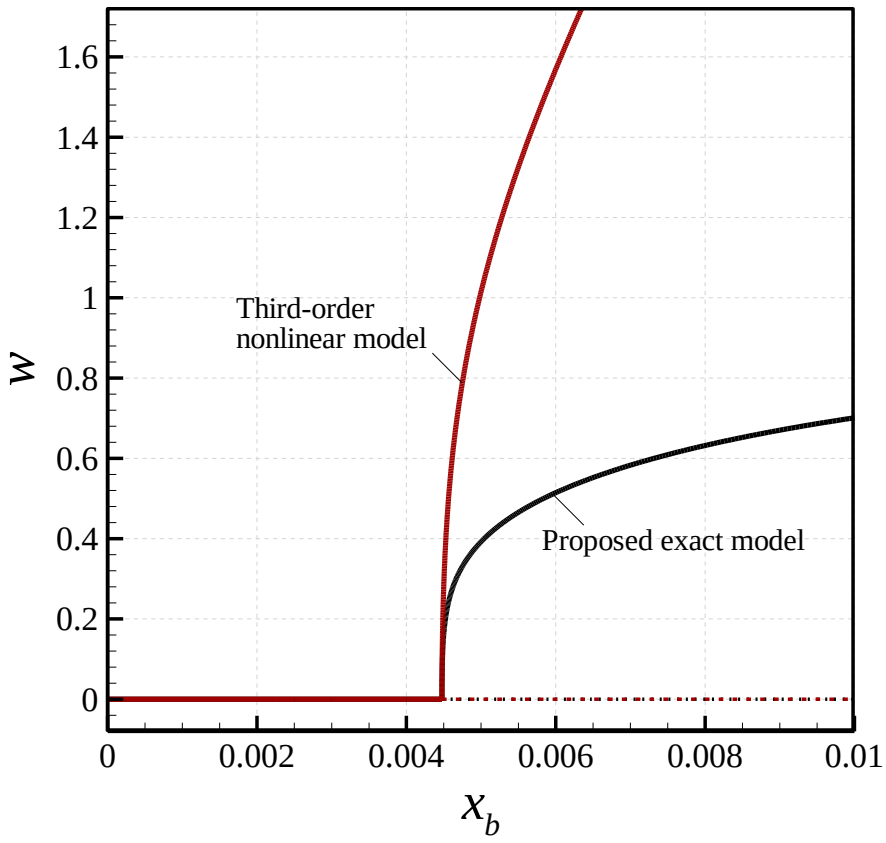

Fig.15. Comparison of large-amplitude responses of the cantilever obtained using the proposed model and a third-order model of the transverse motion of the cantilever. (a) static response under a tip load in *z* direction; (b) parametric resonance response when ω_b/ω_1=2.0.